Research Article

Synthesis, characterization and in vitro cytotoxicity study of Co and Ni ferrite nanoparticles prepared by sol-gel method

Alexandre Pancotti[1] · Dener Pereira Santos[1] · Dielly Oliveira Morais[1] · Mauro Vinícius de Barros Souza[1] · Débora R. Lima[1] · Valcinir Aloisío Scalla Vulcani[1] · Alessandro Martins[1] · Richard Landers[2] · Alexandre Braoios[1]

Received: 13 April 2021 / Accepted: 21 June 2021
Published online: 30 June 2021

Abstract
In this study, we report the synthesis and characterization of $NiFe_2O_4$ and $CoFe_2O_4$ nanoparticles (NPs) which are widely used in the biomedical area. There is still limited knowledge how the properties of these materials are influenced by different chemical routes. In this work, we investigated the effect of heat treatment over cytotoxicity of cobalt and niquel ferrites NPs synthesized by sol-gel method. Then the samples were studied using transmission electron microscopy (TEM), X-ray diffraction (XRD), X-ray photoelectron spectroscopy (XPS), vibrating sample magnetometer (VSM), Fourier Transform Infrared Spectroscopy Analysis (FTIR), and X-ray fluorescence (XRF). The average crystallite sizes of the particles were found to be in the range of 20–35 nm. The hemocompatibility (erythrocytes and leukocytes) was checked. Cytotoxicity results were similar to those of the control test sample, therefore suggesting hemocompatibility of the tested materials.

Keywords X-ray photoelectron spectroscopy · X-ray fluorescence · Nanoparticle · $NiFe_2O_4$ · $CoFe_2O_4$. XPS · PACS number

1 Introduction

Nanotechnology has been widely studied in recent decades due to the novel properties of materials at small scale. For example, nanometers scale magnetic nanoparticles (mNPs) show some positive and fascinating possibilities for applications in health area [1]. For mNPs with controlled size and shape, going from a few nanometers up to 30 nm, nanoparticles demonstrate many new usages and shed light on a variety of applications, such as controlled heating in areas with tumorous tissues [1]. The reduced size of mNPs is particularly important when compared to the size of bio-units, for example, cell, virus, protein, etc. Due to their small size, nanoparticles could be coated with biological molecules [2], thus enabling the interaction or binding to a biological entity, providing controllable means for a "biological marker" [2]. For medical applications, nanoparticles should have specific properties such as a small size which is less than 50 nm. The main challenge for magnetic nanoparticles is their rapid agglomeration. To avoid this, nanoparticles are normally coated with several polymers such as dextran, chitosan, poly ethylene glycol (PEG), and poly vinyl alcohol. mNPs can be manipulated by external magnetic fields [3] which enable a remote control at a large distance. Combined with the large penetration capability of magnetic fields in human tissues, mNPs offer many applications related to the transportation and/or immobilization of nanoparticles, as well as biological entities with magnetic markers [4, 5] which gives an alternative

✉ Alexandre Pancotti, apancotti@ufg.br; apancotti@gmail.com | [1]Unidade Acadêmica Especial de Ciências Exatas e Tecnológicas, Universidade Federal de Jataí, Rod. Br 364, km 168, CEP 75801-615 Jataí, GO, Brazil. [2]Universidade Estadual de Campinas, Instituto de Física Gleb Wataghin, CEP 13083-859 Campinas, SP, Brazil.

way to carry anticancer drugs to specific regions of the human body with tumor cells.

Alternating magnetic fields can transfer energy to the nanoparticles, allowing the controlled heating of mNPs at the regions with tumors. Due to this special physical properties of mNPs, we may observe more effective results than chemotherapy and radiotherapy. To consider the various possibilities of using mNPs in the nanometer scale, a systematic study of how to fabricate, characterize, manipulate and organize these kinds of materials is necessary. This could also reveal the novel properties of nanomaterials differing from that in "bulk" [6, 7]. Given the importance of the study involving materials at nanometric scale, this study contributes to the knowledge of the characteristics of nickel ferrite $NiFe_2O_4$ and cobalt ferrite $CoFe_2O_4$, and presents data on hemocompatibility of these materials, contributing to future applications in the biomedical field.

Nanoparticles of transition metal oxides such as cobalt ferrite ($CoFe_2O_4$) and nickel ferrite ($NiFe_2O_4$) show many excellent optical, magnetic and electrical properties and have been widely applied in a variety of industries, e.g. information storage devices, energy storage facilities, catalysts, etc. [8].

$CoFe_2O_4$,besides its excellent chemical stability [9], is known as a hard magnetic material with high coercivity and moderate magnetization [9]. On the other hand, $NiFe_2O_4$ is a type of soft magnetic material, with low coercivity [10] and low saturation magnetization [1]. Both hard and soft nanoparticulate materials have different biological applications such as bio-sensors, drugs carriers, or contrast agents in magnetic resonance [11]. Different synthesis techniques for $CoFe_2O_4$ and $NiFe_2O_4$ nanoparticles are reported, for example, sol-gel method, evaporation, condensation, microemulsion, combustion, spray pyrolysis, hydrothermal, etc. [12–15]. The polymeric precursor method involves a sol-gel process, which starts with precursors in the liquid state, followed by the formation of the Sol phase, which is a colloidal suspension, for the gel phase. Organic precursors that have a chelating function are used to form the gel, which may be citrate (citric acid), gelatin, coconut water, etc. The final product is heat treated to form stable and homogeneous crystalline structures. In the normal sol-gel synthesis of $CoFe_2O_4$ and $NiFe_2O_4$ mNPs, the gel phase is the result of chemical bonding between the chemical species.

Nanoparticles should have low toxicity and high biocompatibility for medical applications. However, the toxicity of nanoparticles is one of the limiting factors for their successful application in the biological area. There is still very little knowledge of how the physical and chemical properties of these materials are influenced by different chemical routes. In this paper, we studied the effect of different heat treatment temperatures on the cytotoxicity of Co and Ni ferrites NPs, prepared by sol–gel method.

It has been known that the toxicity of nanoparticles is related to the surface area of the NPs and it may be expected that small-sized NPs with more surface area are more toxic to the cells than large-sized NPs. For example, the toxic effect for CeO_2 NPs was related to with increased oxidative stress [16, 17]. On the other hand, the antioxidant effect of CeO_2 NPs plays a protective role in the body by eliminating free oxygen radicals [18]. However, the toxicity of nanoparticles is one of the limiting factors for their successful application in medicine. Though iron oxide nanoparticles without any covering proved to be toxic, recent studies on cytotoxicity in iron oxide nanoparticles coated with thiol type hydrophobic ligands have shown they are non toxic in human lymphocytes [5, 19]. Nowadays, surface-coating of nanoparticles offers a unique strategy to modulate the toxicity [15]. Even though many studies have focused on the biomedical applications of $CoFe_2O_4$ and $NiFe_2O_4$ NPs, there are few studies in the literature that relate the changes in the physical chemical properties of these materials with the cytotoxicity of nanoparticles. Nanoparticles formed by gold and silica have shown to be biocompatible with blood cells [20, 21]. Bohara, et al. [21] reported that $CoFe_2O_4$ nanoparticles coated with amine have no toxic effect on MCF7 (human breast cancer cell line) and L929 (mouse fibroblast). In another study, Momi et al. [5] reported that nanoparticles of cobalt-zinc ferrite coated with DMSA are non toxic for prostate cancer cells. However, to our knowledge, there is very few work related to the toxicity of nickel and cobalt ferrites in the literatures [22–24, 48].

In this study, we introduce a different sol-gel method, where the solution containing the required cations was mixed with colorless gelatin, forming a polymer network with the cations connected to that monomeric network. This polymer network enables the structural formation for the controlled growth and morphology of these mNP, which demonstrate good magnetic properties. The main characteristics of $CoFe_2O_4$ and $NiFe_2O_4$ are studies. The mNP were characterized with X-ray Diffraction (XRD), X-ray Fluorescence (XRF), Transmission Electron Microscopy (TEM), X-ray Photoelectron Spectroscopy (XPS), Fourier Transform Infrared Spectroscopy Analysis (FTIR), and vibrating sample magnetometer (VSM).

We also present hemocompatibility test of these materials, where *in vitro* cytotoxicity tests for the nanoparticles were performed. To our knowledge, this is the first experimental work reporting the upper limits of concentration of cobalt and nickel ferrite on horse blood cells.

2 Experimental methods

2.1 Synthesis of $NiFe_2O_4$ and $CoFe_2O_4$ nanoparticles

The $NiFe_2O_4$ and $CoFe_2O_4$ ferrite nanoparticles were prepared by using the sol-gel method, with a molar ratio of 1:2 (Co:Fe or Ni:Fe). To obtain the cobalt ferrite, 20.655 g of $Fe(NO_3)_3.9H_2O$ and 7.44 g of $Co(NO_3)_2.6H_2O$ were weighed. To obtain nickel ferrite, 20.655 g of $Fe(NO_3)_3.9H_2O$ and 7.40 g of $Ni(NO_3)_2.6H_2O$ were weighed. Each salt was added, separately, in 90 mL of distilled water. And in another 4 containers, 10.341 g of colorless gelatin was added in 90 mL of distilled water. The metal salts and gelatine were kept under constant stirring and heating at 40 °C for 40 min. After complete dissolution, the gelatin and each nitrate were mixed separately, keeping under constant stirring and heating. After dissolution, the iron nitrate and gelatin solutions were mixed with the cobalt nitrate solution. After this step, the resulting solution was placed in a drying and sterilization oven at a temperature of 100 °C for 24 h to evaporate the water. After drying, the samples formed the xerogel and were macerated until the formation of a homogeneous powder. The powders were divided into four fractions to be heat treated in a tubular oven at different temperatures between 250 and 1000 °C, with a heating rate maintained at 4 °C/minute. The heat treatment was maintained for 4 h after reaching the set temperature, and then left to cool to room temperature. Finally, the removal of residual organic matter was carried out by chemical treatment with 35 % H_2O_2, for a few minutes. The material was washed with distilled water, followed by centrifugation, to separate the supernatant from the synthesized material. At the end of the synthesis, the nanoparticle formed was placed to dry at a temperature of 120 °C for 24 h [7].

The heat treatment of the $NiFe_2O_4$ NPs done at following temperatures, 250 ºC, 500 ºC, 800 ºC and 1000 ºC and for the $CoFe_2O_4$ NPs at 250 ºC, 600 ºC, 800 ºC and 1000 ºC.

2.2 Intrumentation

The XRD technique was used in order to identify the presence of phases in the sample and checking the crystallinity of the nanoparticles. The XRD experiments were measured at XRD1 beamline of the National Synchrotron Light Laboratory (LNLS). The detection system consists of a linear arc of 25 detectors, enabling measurements with a step 0.004º, in a range of 121°. The radiation used was generated by a double crystal silicon monochromator, with a wavelength equal to 1.034 Å.

The XPS spectra were collected using a conventional Al K_α X-rays source with photon energy of 1486.6 eV. A VSW HA100 electron analyzer was used with 44 eV pass energy and 0.1 eV step. The base pressure in the analysis chamber was less than 5.0×10^{-9} mbar. The binding energy (BE) scale was calibrated using the C 1 s line at 284.6 eV as a reference. A 30° takeoff angle was used to increase the surface sensitivity of the core level peaks. The data was analyzed using the Winspec software. Shirley backgrounds were subtracted from the experimental data results.

The size distribution histogram of the $NiFe_2O_4$ and $CoFe_2O_4$ NPs was obtained through TEM analyses which were carried out with an electron microscope operating at an accelerating voltage of 100 kV (JEOL JEM-2100 EXII).

In order to characterize the composition, and concentration between the atoms in the formed ferrites, the X-Ray Fluorescence (XRF) was used to study the NPs. The XRF measurements were performed on a Ray Ny EDX-720 Shimadzo equipment.

To perform the FTIR, it was necessary to prepare samples in the form of pellets, mixing the following quantities : 1 % in mass of the NPs and 99 % of the potassium bromide (KBr), and pressing in a thin insert. The simple was placed in the JASCO FTIR-4100 sample holder. Data acquisition was performed in the range of 400 to 4000 cm-1 with 0.01 cm^{-1} of step. The results were plotted using the Spectra Manager software.

The VSM measurements for the magnetic sample were recorded with a PAR-EGG (model 4500) platform. Each sample was mounted on the top of the vibrating probe kept between two magnetic poles and continuously vibrated mechanically during the analysis. The applied magnetic field was gradually increased from 0 to 20.000 Oe, then it was reduced to – 20.000 Oe, and again increased to 20.000 Oe to complete the hysteresis loop.

2.3 Cytotoxicity measurements

The samples were sterilized using 20 % ethylene oxide for 6-hour with an average pressure of 0.750 kgf·cm^2, at 55 °C temperature and an average humidity of 60 %. ATTEST RAPID 1294 (lot 2016-08TD) was used as a biological indicator and multiparametric tape for ethylene oxide (lot 2015-01AA) as a chemical control. The hemocompatibility of the nanoparticles were evaluated by tests using blood of healthy horses that had no hematologic and leukocyte changes.

Hemoglobin release was assessed using photon spectrophotometry of Ultra-Violet-Visible, with a wavelength of 540 nm, which permits assess to the amount of free hemoglobin. Hemoglobin is an oxygen-carrying protein that is inside red blood cells. When there is hemolysis (rupture

of the red cell membrane), the amount of hemoglobin released is detected. Biomaterials designed to interact directly or indirectly with blood must be subjected to the hemolysis test. An elevated plasma hemoglobin level reflects erythrocyte membrane fragility in contact with materials and devices. For this, the measured absorbance was associated with the amount of hemoglobin released into the blood.

Firstly, the volumetric condition of the blood cells was verified using 5 mL of horse venous blood, that was centrifuged for 10 min at 2500 rpm to separate plasma fom the red blood cells. The plasma was removed by aspiration and the same volume of phosphate buffered saline solution was added to the test tube. This process was repeated three consecutive times. Subsequently, the globular volume was adjusted to 5 % by diluting 2.5 mL of red blood cells in 47.5 mL of glycophysiological serum, 10 µL of penicillin (30 mg/mL) and 10 µL streptomycin (50 mg/mL).

For each of the heat treated samples, four solutions with concentrations of 0.02, 0.2, 1.2 and 8 mg/mL were prepared with 50 mL of phosphate buffered saline solution. Sequencialy, 100 µL of each solution was added to 4900 µL of packed red blood cells in a test tube. As a control 100 µL of pure phosphate buffered saline was also added to the same amount of red blood cells.

The tubes were incubated at 38 ºC in an oven, under constant agitation at approximately 50 rpm. After 24 h of incubation, the tubes were centrifuged for five minutes at 4000 rpm, to then be tested for hemoglobin release.

We evaluated the hemolysis rate and cell viability of leukocytes by staining with trypan blue. For this, 5 mL of equine venous was used. 2 mL of plasma expander were added, the solution was kept for 20 min in an oven at 38 °C, with a 45 ° inclination to favor the precipitation and separation of red blood cells and leukocytes.

Subsequently, the plasma and leukocytes were removed by aspiration, and transferred to another test tube and centrifuged for 10 min at 2500 rpm. Thus, the leukocytes formed pellets and the supernatant was discarded so that the leukocytes could be resuspended in 2 mL of 0.9 % saline solution. Turk's solution (1:20) was added to promote the lysis of remaining red cells and platelets. Then, 20 µL of the NPs solutions was pipetted and added in eppendorfs containing 980 µL of the leukocyte concentrate. For the control assay, 20 µL of phosphate buffered saline and 980 µL of leukocyte concentrate were also prepered. To determine cell viability, the test and control solutions were incubated for 6 h at 38 ºC with constant agitation of 50 rpm.

Subsequently, 1.5 % Tripan Blue dye was added in the same proportion as the solution. After three minutes, the leukocyte count was performed in a Neubauer chamber. Leukocytes that incorporated the blue dye were counted as non-viable cells, that is, they suffered damage to the membrane, and those that did not incorporate the dye, were counted as viable cells.

As described above we performed hemocompatibility tests on eight samples, four different concentrations (0.02, 0.2, 1.2 and 8 mg/mL) for $NiFe_2O_4$ and $CoFe_2O_4$ NPs. The hemolysis rate and cell viability of leukocytes was evaluated by staining with trypan blue.

Blood samples and *in vitro* cytotoxicity experiments were approved by the Ethics Committee on Animal Use, Protocol 041/15 of 09/14/2015. The tests were analyzed in triplicate and a statistical analysis was performed using analysis of variance (ANOVA) followed by Dunnett's test (multiple comparisons to a single control with $p < 0.05$).

3 Results and discussion

3.1 Electronic and Structural Properties of the Nanoparticles

3.1.1 TEM

Firstly we have performed the sol-gel proteic synthesis of $CoFe_2O_4$ and $NiFe_2O_4$ NPs, accompanied of the heat treatment of these NPs at different temperatures in order to probe its effects over their crystallinities, particle size, surface composition, magnetic properties, and cytotoxicity. Here as we are interested in investigating the particle size and surface morphology over the cytotoxicity of nanoparticles, we want to present the heat treatment effect at 800 °C on $CoFe_2O_4$ and $NiFe_2O_4$ NPs.

Figure 1 shows TEM images of the NPs heat treated at 800 °C for 4 h. Figures (a) and (b) for $CoFe_2O_4$, scale bars of 140 nm and 5 nm, respectively. Figures (d) and (e) are for $NiFe_2O_4$ NPs, scale bar of 100 nm and 10 nm, respectively. Their corresponding size histograms are depicted for $CoFe_2O_4$ (c) and $NiFe_2O_4$ nanoparticles in figures (c) and (f). To obtain the histogram a total of $N = 300$ different particles sizes were used. Subsequently, a particle size histogram was mounted using the Sturges method [25]. The width (W) was obtained from the relation: $W = (Dmax - Dmin)/k$, where $k = 1 + 3.322 \log(N)$. The histogram is fairly well modeled by a log-normal distribution, as shown in Fig. 1(c,f).

The histogram shows a Lorentzian distribution with mean diameter of 33.5 nm for $NiFe_2O_4$ and 29.0 nm for $CoFe_2O_4$ NPs, respectively. The TEM images obtained for $CoFe_2O_4$ and $NiFe_2O_4$ NPs that were heat treated at 250 °C showed characteristics of amorphous material. For this reason, their corresponding TEM images are not shown here. In general, the NP size were smaller to the samples heat treated at low temperature when compared to NPs

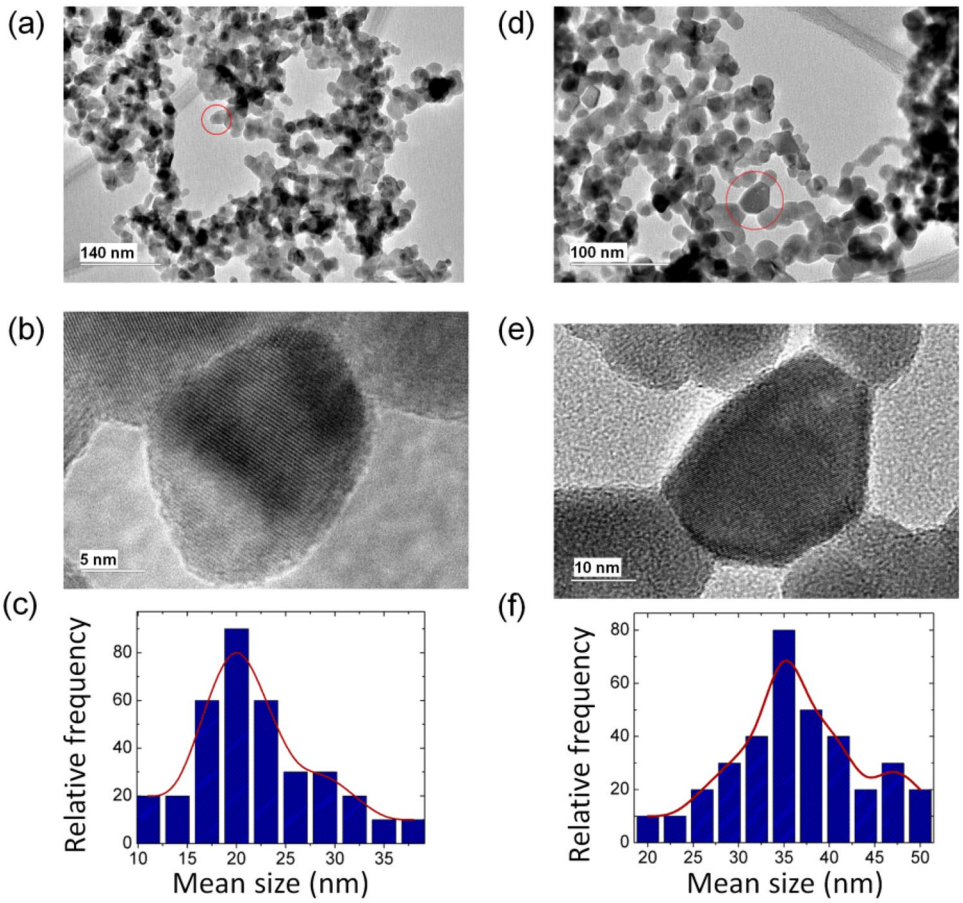

Fig. 1 TEM images for $CoFe_2O_4$ NPs after heat treated at 800 °C obtained at 140 nm (**a**) and 5 nm scale bar (**b**), TEM images for $NiFe_2O_4$ NPs after heat treated at 800 °C obtained at 100 nm (**d**) and 10 nm scale bar (**e**). Size distribution for $CoFe_2O_4$ (**c**) and $NiFe_2O_4$ nanoparticles after heat treated at 800 °C (**f**)

heat treated at high temperatures. These results are in perfect agreement with the XRD experiment.

3.1.2 XRD characterizations

Figure 2 present the XRD results of samples obtained by the protein sol-gel method. Figure 2a shows the XRD results of $CoFe_2O_4$ heat treated at different temperatures. The formation of the crystalline phase of the $CoFe_2O_4$ started at 250 °C. For the heat treatment at higher temperatures (800 and 1000 °C), the diffraction pattern became more intense, which indicates better crystalline quality[27, 48, 51]. The average values for the most intense reflection obtained for the lattice parameter constant was 8.39 Å. It has been reported by Fontanive [26] et al. that the $CoFe_2O_4$ mNPs heat treated at 400 °C showed a secondary phases during formation. However, in this study, only a single phase was observed. The results are consistent with those reported by Goncalves, et al. [27], where $CoFe_2O_4$ only demonstrates one phase even heat treated at 1000 °C.

Figure 2b shows that for annealing temperatures above 800 °C NPs of $NiFe_2O_4$ formed with high crystallinity. XRD data further revealed a cubic spinel structure, where the unit cell of $NiFe_2O_4$, is a face-centered cubic (FCC). In addition, a detailed analysis of the diffraction pattern demonstrates that only one phase exist in heat treated $NiFe_2O_4$ samples. The average values for the most intense diffraction peakss obtained for the lattice parameter constant was 8.32 Å, this value confirms the $NiFe_2O_4$ formation [21, 24–30].

Table 1 Crystallite sizes (nm), where the 2θ was obtained from the XRD diffractograms. We have used the constant k = 0.91 and λ = 1.54 Å in the Scherrer Equation

Bragg angle 2θ	Miller indices	Ni800 °C	Ni1000 °C	Co250 ° C	Co800 °C
36°	311	13.0	35.9	17.1	25.4
41°	400	25.2	41.3	26.5	35.3
50°	422	20.1	38.0	23.3	38.9
53°	511	19.9	41.1	25.2	36.8

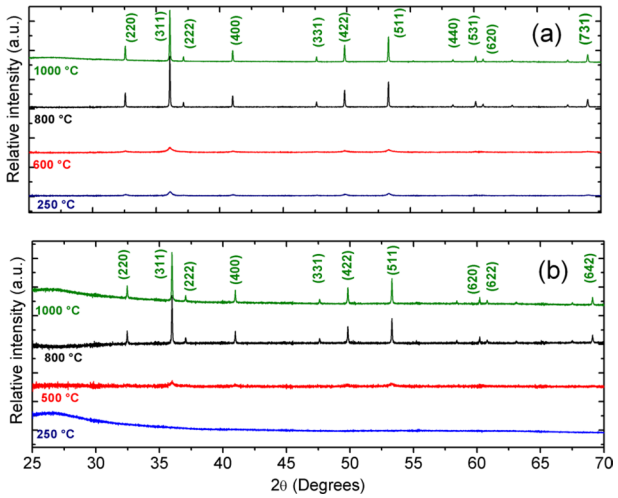

Fig. 2 XRD diffractograms for **a** $CoFe_2O_4$, **b** $NiFe_2O_4$ heated at different temperatures

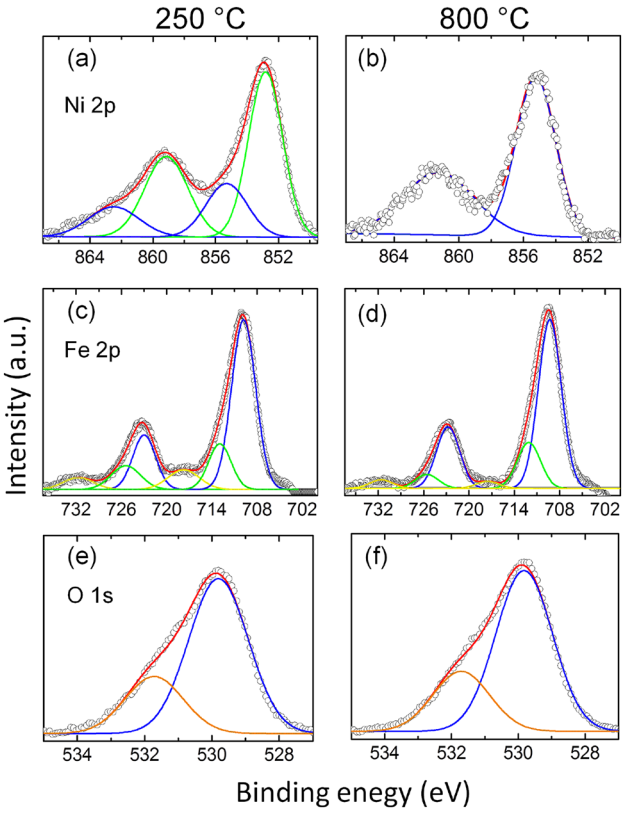

Fig. 3 XPS Core-level spectra for Ni ferrite nanoparticles heat treated at 250 and 800 °C for :**a**,**b** Ni 2p; **c**,**d** Fe 2p; **e**,**f** O1s

Table 1 shows the crystallites sizes for the synthesized Nps. The crystallites sizes were determined by Scherrer Equation.

The Table 1 show that cristallite sizes changed after the hight temperature heat treatment. We observed that higher heat treatment temperatures produce higher intense diffractions, increased grain size and better crystallinity. We beleave that the size of the NP has a great influence on cytotoxicity effect.

3.1.3 XPS

To study the information on the composition of the NPs as a function of the heat treatment treatment, we have done the XPS analyses on the $NiFe_2O_4$ and $CoFe_2O_4$ NPs heat treated at two different temperatures, at 250 and 800 °C.

The Ni 2p, Fe 2p, and O 1 s core-level XPS spectra of $NiFe_2O_4$ NPs heat treated at 250 and 800 °C are shown in Fig. 3. In the Fig. 3a, the Ni $2p_{3/2}$ core-level of $NiFe_2O_4$ NPs heat treated at 250 °C spectra has 2 components, with binding energy (BE) of 852.9 eV and 855.6 eV corresponding to octahedral and tetrahedral sites [31–34], respectively, with their shake-up satellites at 859.2 eV and 862.5 eV.

Figure 3b shows the Ni $2p_{3/2}$ core-level of $NiFe_2O_4$ NPs heat treated at 800 °C. The peaks with BE equal to 855.4 eV and 861.3 eV refer to the main peak and satellite peak, respectively. The octahedral site is favored the in this case.

The XPS spectrum of Fe 2p core-level heat treated at 250 °C are presented in Fig. 3c. For Fe^{3+} ions, the Fe $2p_{3/2}$ spectrum can be divided into 3 components. The components with BE of 709.6 eV and 712.6 eV indicate Fe^{3+} ions present in the tetrahedral and octahedral site of spinel structure, respectively. The high binding energy HBE component with BE of 717.6 eV might be the shake-up satellite structure of tetrahedral and octahedral ions [35]. For Fujii, et al. [35], there is a satellite shake-up structure in the XPS spectra for the tetrahedral and octahedral ions around 717.7 eV for Fe $2p_{3/2}$ and 731.6 eV for Fe $2p_{1/2}$. The author also reports that the XPS spectra of Fe $2p_{3/2}$ level from phase γ-Fe_2O_3 is very similar to nickel ferrite, while Fe_3O_4 has satellite structures around 714 eV to 720 eV [32]. For Fujii, the position of the 2p peak of the Fe for Fe^{2+} ions is around 712.7 eV and 710.5 eV for the tetrahedral and octahedral sites.

Figure 3d shows the XPS spectra of Fe 2p core-level heat treated at 800 °C. There is only one component due to the formation of the octahedral site as mentioned previously.

Figure 3e presents the XPS spectra of O 1 s core-level heat treated at 250 °C. There are 2 components in this spectrum. The component with BE of 527.5 eV, corresponding to oxygen in the bulk structure. The component with BE of 529.4 eV ascribed to carbonate or hydroxyl groups chemically bound to surface cations of NPs [34, 36]. The values of binding energy for the O 1 s are very close to the values reported by Zhao, et al. [34].

Figure 3f shows the XPS spectra of O 1 s core-level heat treated at 800 °C. The peaks with BE equal to 529.8 eV and 531.7 eV refer to the bulk structure and adsorption bound to surface cations as discussed before. The difference of BE O 1 s core-level for the $NiFe_2O_4$ samples heat treated at 250 and 800 °C could correspond to differences in crystallinity.

Figure 4a, shows the XPS spectra of Co $2p_{3/2}$ core-level heat treated at 250 ° C, which has three components with BE of 779.6 eV, 782.4 eV and 786.3 eV. The BE of 779.6 eV and 782.4 eV were related to Co^{2+} ions in the octahedral and tetrahedral sites [9, 34]. The peak with BE of 786.3 eV corresponding to the shake-up satellite peak of Co $2p_{3/2}$ main line [9, 37].

The Co $2p_{3/2}$ core-level of $CoFe_2O_4$ NPs heat treated at 800 °C is presented in Fig. 4b. The XPS spectrum also also has 3 components with BE of 781.1 eV, 784.0 eV and 788.2 eV. The components present in 781.1 eV and 784.0 eV were associated with Co^{2+} ion in octahedral and tetrahedral sites. The binding energy of 788.2 eV corresponds to the shake-up satellite peak [9, 37].

Figure 4c shows the Fe 2p core-level of $CoFe_2O_4$ NPs heat treated at 250 °C. Here, the spectrum has 3 components. The BE of 709.4 eV (Fe $2p_{3/2}$) and 722.9 eV (Fe $2p_{1/2}$) refers to the Fe^{3+} ions in octahedral site, with corresponding satellite peaks at 717.3 eV (Fe $2p_{3/2}$) and 731.2 eV (Fe $2p_{1/2}$), respectively. The BE of 712.2 eV and 725.5 eV, was related to Fe^{3+} ions in tetrahedral sites.

Figure 4d presents Fe 2p core-level of $CoFe_2O_4$ NPs heat treated at 800 °C. The spectrum has 2 components with BE of 711.3 and 714.0 eV. The peak with BE of 711.3 eV corresponds to the Fe^{3+} ions in octahedral site, and the BE of 714.0 eV corresponds to Fe^{3+} ions in tetrahedral site as shown in the Fig. 3d.

Figure 4e shows the O1s core-level of $CoFe_2O_4$ NPs heat treated at 250 °C, which has 2 components with BE of 530.0 eV and 528.5 eV. Similar to the the $NiFe_2O_4$ NPs mention previously, the component present at 530.0 eV was attributed to oxygen of bulk structure and the component at 528.5 eV was associates to carbonate or hydroxyl groups chemically bound to surface cations of NPs.

Figure 4f shows the XPS spectrum of the O 1 s core-level heat treated at 800 °C. Like that of $NiFe_2O_4$ NPs, the components with BE of 528.0 eV associates to the bulk structure and the BE of 530 eV is ascribed to adsorption bound to surface cations of NPs.

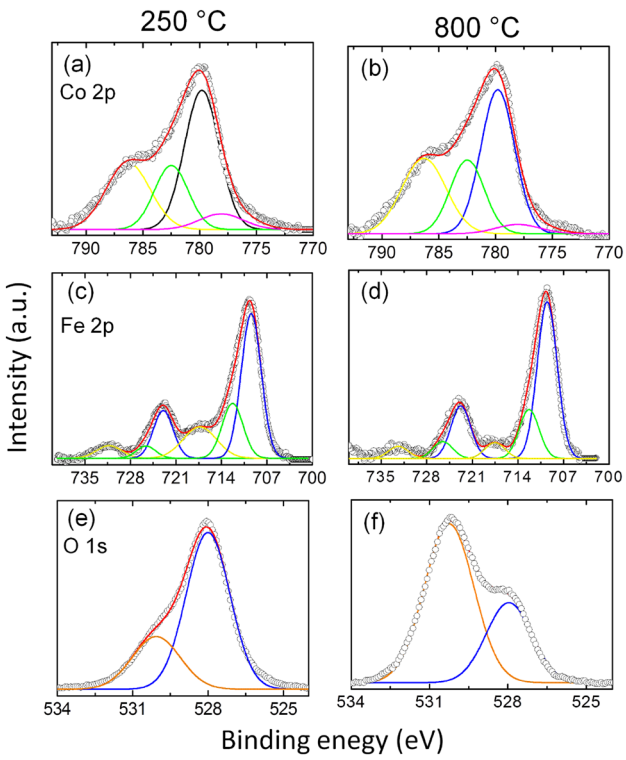

Fig. 4 XPS Core-level spectra for Co ferrite nanoparticles heat treated at 250 and 800 °C for : **a**,**b** Co 2p; **c**,**d** Fe 2p; **e**,**f** O1s

3.1.4 XRF

In order to obtain details on the composition and concentration, we performed XRF analysis of the Nps. Figure 5 shows a typical XRF spectra for the (a,b) $CoFe_2O_4$ heat treated at 250 and 800 °C and (c,d) $NiFe_2O_4$ Nps heat treated at 250 and 800 °C. The average chemical composition obtained for the $CoFe_2O_4$ are, respectively: 64.5 %-wt (63.0 %-wt) Fe, 32.9 %-wt (32.7 %-wt) Co. The components present at 6.9 keV and 7.5 keV ((Fig. 5(a,b)) were associated to K_α and K_β line of the Co atom. The components present at 6.4 keV and 7.0 keV ((Fig. 5(a,b)) were associated to K_α and K_β line of the Fe atom. These concentrations are compatible with the amounts of elements used during the preparation process of the Nps. Thus, according to the expressed results in percentage concentration, shown in Fig. 5, it was possible to verify that the stoichiometric ratio of 2:1 (iron and metal ion) corresponds to ferrite with the following stoichiometry $CoFe_2O_4$. The elements obtained in low concentrations are due to the use of gelatin as a precursor. Concentrations below 5 % not affected the crystalline structure of Np synthesized. In the similar experimental experiment performed by Yoon et al. [38], a percentage concentration for zinc ferrites was determined, with the XRF technique, equal to 71.3 %-wt Fe and 28.7 %-wt Zn, maintaining the same ratio equal to 2:1 (Fe:Zn). In other studies [39], also using the XRF technique, for mixed zinc and magnesium ferrites it was shown that the peaks present at energies equal to 6.49 keV and 7.15 keV were associated with Fe atoms, and the peaks present at equal energies at 8.68 keV and 9.57 keV were associated with

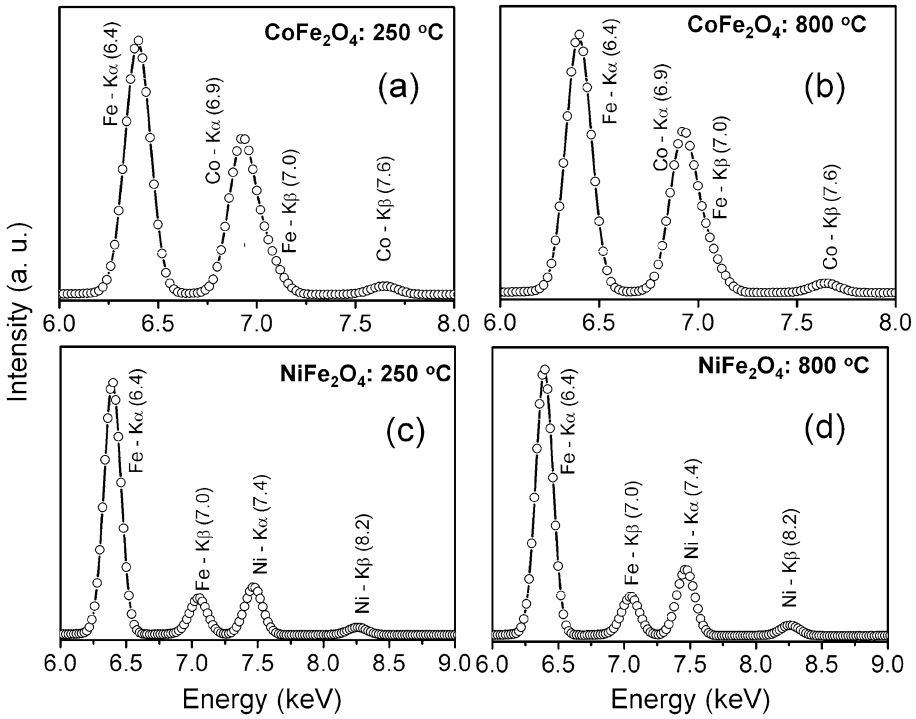

Fig. 5 XRF Spectra analysis of the $NiFe_2O_4$ and $CoFe_2O_4$ NPs: **a** $CoFe_2O_4$ heat treated at 250 °C; **b** $CoFe_2O_4$ heat treated at 800 °C; **c** $NiFe_2O_4$ heat treated at 250 °C and **d** $NiFe_2O_4$ heat treated at 800 °C

Zn atoms[39]. These values obtained by the mentioned author are similar to those reported in this work.

The average chemical composition obtained for the $NiFe_2O_4$ are, respectively: 66.7 %-wt (61.8 %-wt) Fe, 28.7 %-wt (34.8 %-wt) Ni. The components present at 7.4 keV and 8.2 keV ((Fig. 5(c,d)) were associated to K_α and K_β line of the Ni atom. The components present at 6.4 keV and 7.0 keV ((Fig. 5(c,d)) were associated to K_α and K_β line of the Fe atom. Other elements of small proportions Fig. 5 have been identified and they can be attributed to the use of commercial gelatin in the Sol-Gel-Protein method.

3.1.5 FTIR

Figure 6 exhibits the typical FTIR spectrum of $CoFe_2O_4$, and $NiFe_2O_4$ NPs heat treated at two different temperatures, which exhibits various well-defined peaks. Figure (a) shows the absorption peaks for $CoFe_2O_4$ calcined at 250 °C and (b) at 800 °C. The peaks at 416 cm^{-1} (420 cm^{-1}), 592 cm^{-1} (587 cm^{-1}), 1120 cm^{-1}(1085 cm^{-1}), 1398 cm^{-1} (1401 cm^{-1}), 1638 cm^{-1} (1628 cm^{-1}) and 3461 cm^{-1} (3442 cm^{-1}) were associated with the chemical bonds between the atoms of Fe-O, Co-O or Fe-O, C = O, C-H, O-H, and O-H, respectively. Figure (b) shows the absorption peaks for $NiFe_2O_4$ heat treated at 250 °C and (d) at 800 °C. The band at 550 cm^{-1} represents the tetrahedral mode of $NiFe_2O_4$, respectively. The band located at 3390 cm^{-1} could be attributed to the symmetric vibration of -OH groups. The bands with peaks observed at 1040 cm^{-1} could be assigned to O-H bending vibration.

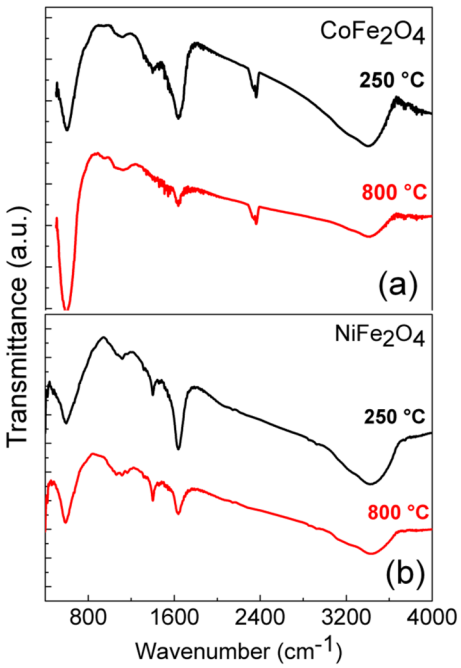

Fig. 6 Typical FTIR spectrum of calcinated nanoparticles. FTIR spectroscopy of **a** $CoFe_2O_4$, **b** $NiFe_2O_4$ calcined at 250 and 800 °C

3.1.6 VSM

Figure 7(a,b) shows the hysteresis curves of $NiFe_2O_4$ NPs heat treated at 250 °C (remanence Mr = 0.01 emu/g and coercive field Hc = 0.06 kOe) and 500 °C (Mr = 1.22 emu/g

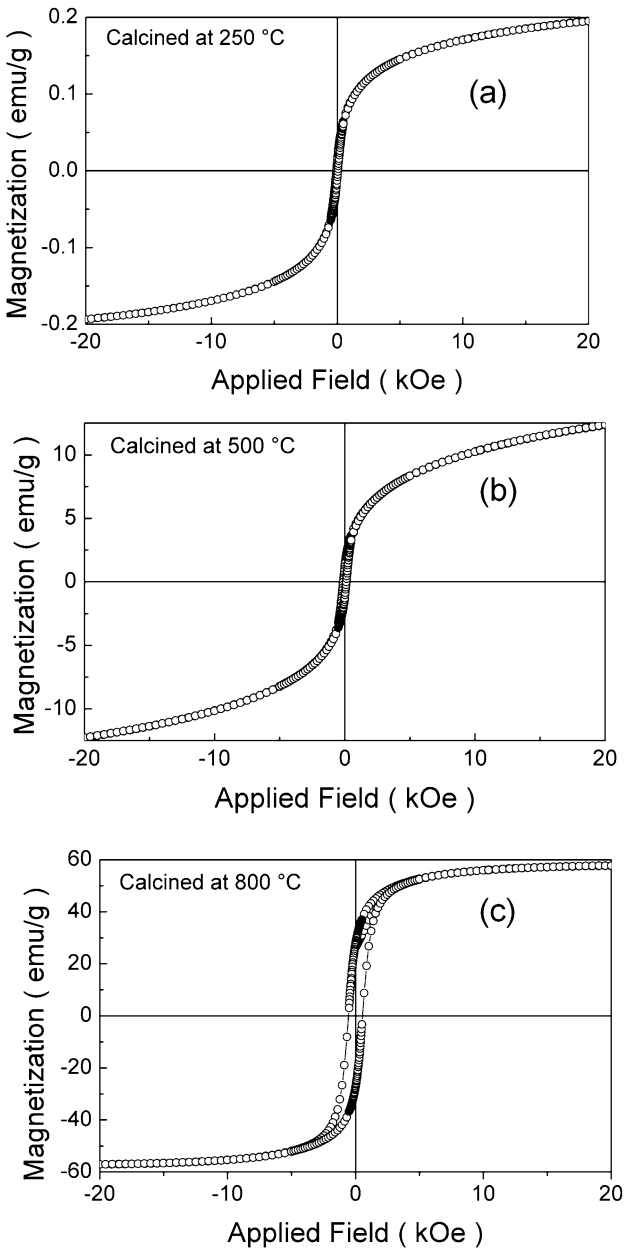

Fig. 7 Hysteresis curves of $NiFe_2O_4$ heat treated at 250 °C **a** and 500 °C **b** $CoFe_2O_4$ heat treated at 800 °C. The samples were analyzed at room temperature

and Hc = 0.12 kOe). The higher values of remanence and coercive field in the sample heat treated at 500 °C reveals growth of crystallinity, in agreement with XRD measurements. The $NiFe_2O_4$ NPs exhibit weak ferromagnetic behavior and suggests superparamagnetic-like behaviors, which is ideal for medical applications [40]. Singh et al. [41] synthesized Ni ferrite nanoparticles with High Energy Ball milling (HEBM) technique, through of the α-NiO and α-Fe2O3 mixture, followed by annealing at 1000 ˚C. The measured saturation magnetization and coercivity for milled followed by annealing nickel ferrite nanoparticles was 36.72 emu/g and 49.65 Oe.

The $CoFe_2O_4$ NPs heat treated at 800 °C demonstrate a Hc = 0,55 kOe and Mr = 0.27 emu/g, which suggests hard magnetic behavior with positive and a much larger magnetocrystalline anisotropy constant behavior at room temperature. Houshiar et al. [42] using three different methods of synthesis, combustion, coprecipitation, and precipitation obtained a saturation point in the magnetic field of less than 15 kOe. For samples synthesized by the combustion technique the magnetization saturation (Ms) measured was 56.7 emu/g and for co-precipitation and precipitation, Houshiar obtained 55.8 emu/g and 47.2 emu/g of magnetization saturation (Ms). Coercivity (Hc) was 2002 Oe for combustion synthesized samples, and 850 Oe for co-precipitation samples, and 233 Oe for precipitation samples.

Table 2 Absorbance values of the erythrocyte solution and $NiFe_2O_4$ materials at different concentrations and the solution control

Concentration (mg/mL)	$NiFe_2O_4$ – 250 °C	$NiFe_2O_4$ – 800 °C	Control
0.02	0.038	0.087	0.059
0.2	0.056	0.089	
1.2	0.060	0.075	
8	0.061	0.080	

3.2 *In vitro* cytotoxicity tests

3.2.1 Hemocompatibility of $NiFe_2O_4$

To assess the biocompatibility NPs, hemocompatibility tests were applied to verify the hemolysis with erythrocytes and leukocytes by the staining/count technique. Different concentrations of NPs (0.02, 0.2, 1.2, 8 mg/mL) were tested. Simultaneously, a control assay was also carried out to investigate the cytotoxic effect on erythrocytes and leukocytes [20].

A study using iron oxide NPs synthesized by different precursors to evaluate the compatibility with human, bovine, caprine and ovine erythrocytes has been reported. Different concentrations were tested with red blood cells (0.25, 0.50, 1.0, and 2.0 mg/mL). The results demonstrated that the effect of NPs in human erythrocytes were similar to that observed for animal red blood cells, demonstrating the possibility of the cytotoxicity comparison between different species [43–46].

Table 2 shows the results of hemoglobin in the presence of $NiFe_2O_4$ NPs suspensions heat treated at 250 °C and 800 °C, as well as control assay without $NiFe_2O_4$ NPs. In the absence of $NiFe_2O_4$ NPs, the absorbance value was 0.059.

For suspension with 0.02 mg/mL $NiFe_2O_4$ NPs that were heat treated at 250 ºC, the absorbance value was 0.038 and with 0.2 mg/mL was 0.056. It is necessary to remember that the control group, in which the erythrocytes remained agitated for 24 h, presented a small amount of erythrocyte hemolysis. The reading of 0.059 was associated to the hemolysis minimum caused by the agitation. This explains why two absorbance values for $NiFe_2O_4$ were lower than the control group. The amount of hemolysis was slightly lower (without statistical difference), demonstrating that there was no influence from the biomaterial. For the highest concentration 8 mg/mL, the absorbance value was 0.061, very close to the control test without significant differences ($p > 0.05$). The results shows that even with high concentrations of $NiFe_2O_4$ NPs, it did not cause lysis of erythrocytes. The suspension with $NiFe_2O_4$ NPs heat treated at 800 °C at different concentrations demonstrated absorbance values of 0.087 with lowest concentration of 0.02 mg/mL until 0.050 to the highest concentration of 8 mg/mL. There were no significant cytotoxic effects differences when compared to the control test ($p > 0,05$).

The study by Cotica et al. [47] tested the compatibility of human erythrocytes with Fe_3O_4 magnetite NPs, where the NPs heat treated at different temperatures (300 and 500 °C) were tested with different concentrations. The absorbance value on the control test was 0.062. For suspension of 1.8 mg/mL, the NPs with heat treatment at 300 °C showed a value of absorbance lower than 0.06, meanwhile, and suspension of same concentration but with Fe_3O_4 NPs heat treated at 500 ºC presenting a value approximately 0.07. For the suspension of NPs with lower concentrations, the results were also similar to our results obtained on $NiFe_2O_4$ NPs. Özçelik et al. [48] studied blood compatibility of nickel nanoferrites prepared by laser ablation technique. The hemolytic activities observed was 1.00 mg/mL and 5.00 mg/mL, lower than obained in this paper. Hemolytic activity was observed at different hypotonic conditions involving different concentration of NPs;In this work we observed that the minimum concentration of NPs inducing hemolysis was 0.05 mg/mL. The Ni ferrites NPs did not inducing hemolysis for higher concentrations.

The results of leukocytes viability $NiFe_2O_4$ NPs heat treated at two different temperatures are presented in Table 3. In the control test the leukocytes viability was 99.97 % (100 – 0.026 %), with no significant differences ($p > 0.05$) with the leukocytes viability of with NPs suspension of different concentration. In all case, the leukocytes viability was greater than 99.95 %.

As for the cytotoxicity test of leukocytes, a study done by Vendrame [49] using magnetite NPs showed a leukocyte cell viability above 95 %. From the results above, there is no cytotoxicity for $NiFe_2O_4$ NPs to leukocytes.

3.2.2 Hemocompatibility of $CoFe_2O_4$

The absorbance values of the hemoglobin released from erythrocytes in the presence of $CoFe_2O_4$ NPs are presented in Table 4. For the suspension with minimum 0.02 mg/mL $CoFe_2O_4$ NPs that were heat treated at 250 ºC, the absorbance value was 0.082. For the highest concentration 8 mg/mL, the absorbance value was 0.147. When compared with the test control, the values showed no statistically significant differences.

For the $CoFe_2O_4$ NPs heat treated at 800 °C, the absorbance values was 0.070 for suspension with minimum 0.02 mg/mL $CoFe_2O_4$ NPs, and for suspension with minimum 8 mg/mL $CoFe_2O_4$ NPs, the absorbance values was 0.062, showing no significant differences with the test control ($p > 0.05$). Absorption values close to or even lower than the control group show that hemolysis was caused by the agitation of blood samples for 24 h. Gajendiran et al. [50] demonstrated that Co ferrite NPs heat treated at 800 ºC have less than 5 % hemolysis, representing a highly hemocompatible nature.

All the results above suggest the material compatibility with the erythrocytes.

The results of the cell viability of leukocytes in contact with $CoFe_2O_4$ NPs are presented in Table 5 and demonstrate that the cell viability of leukocytes were superior to 99.96 % at all tested concentrations, with no significant differences ($p > 0.05$).

In the study by Cotica et al. [51] with $CoFe_2O_4$ synthesized by thermal decomposition heat treated at 400 ºC, the

Table 3 Percentage of leukocyte lysates in control test analysis suspension of $NiFe_2O_4$ nanoparticles at different concentrations

Concentration (mg/mL)	$NiFe_2O_4$ – 250 ºC	$NiFe_2O_4$ – 800 ºC	Control
0.02	0.027	0.011	0.026
0.2	0.029	0.019	
1.2	0.032	0.020	
8	0.016	0.010	

Table 4 Absorbance values of erythrocytes solution and $CoFe_2O_4$ materials, in different concentrations and control solution with erythrocytes

Concentration (mg/mL)	$CoFe_2O_4$ – 250 ºC	$CoFe_2O_4$ – 800 ºC	Control
0.02	0.082	0.070	0.059
0.2	0.037	0.080	
1.2	0.056	0.068	
8	0.147	0.062	

Table 5 Percent cell lysates in control test analysis and in contact with the solution of $CoFe_2O_4$ nanoparticles at different concentrations

Concentration (mg/mL)	$CoFe_2O_4$ – 250 °C	$CoFe_2O_4$ – 800 °C	Control
0.02	0.030	0.027	0.026
0.2	0.021	0.020	
1.2	0.020	0.048	
8	0.001	0.030	

size distribution of NPs was between 20 nm and 100 nm. Different concentrations of NPs (0.005, 0.010, 0.020 mg/mL) were tested for human erythrocytes. The results showed that the absorbance values were close to the control test [45, 46]. The same concentrations were tested with leukocytes and showed a cell viability higher than 93 %, having no significant difference with the control test. Our results presented in this study reinforce that $CoFe_2O_4$ NPs have no cytotoxicity to both erythrocytes and leukocytes.

From all of our previous results above, it can be noted that both $NiFe_2O_4$ and $CoFe_2O_4$ NPs are hemocompatible. There is no erythrocytes and leukocytes damage.

4 Conclusions

The synthesis method used was efficient for obtaining $NiFe_2O_4$ and $CoFe_2O_4$ NPs, which was confirmed by a series of electronic and crystallographic characterization. Regarding the composition of $NiFe_2O_4$ and $CoFe_2O_4$ NPs, the results showed that the concentrations of metal ions varied according to the temperature used in the heat treatment of the material. For the formation of nickel or cobalt ferrite, the concentration of Fe ions in relation to Ni/Co ions according to the values obtained by theoretical calculation considering the molar mass of Fe, Ni, Co, and O, shall have the ratio of 1:2 for Ni or Co in relation to Fe. Considering the identified crystallographic planes for $NiFe_2O_4$ NPs, the samples heat treated between 250 and 600 °C have no evident characteristics crystalline order. However, for heat treatment temperatures above 800 °C, the NPs were obtained with a high degree of crystallinity. Unlike $NiFe_2O_4$ NPs, $CoFe_2O_4$ NPs heat treated at 250 °C showed crystalline order and it was also possible to identify characteristic reflections for $CoFe_2O_4$, but at higher temperatures (above 800 °C) we observed the formation of NPs with a high degree of crystallinity, as demonstrated by more intense and narrower reflections. Was observed the presence of Fe ions in the tetrahedral and octahedral sites, characteristic of spinel-type structures. The Ni ion has also occupied the two sites. The binding energy of the O peaks indicated defects or adsorption of oxygen in the NPs. In $NiFe_2O_4$ NPs heat treated at 800 °C, the Fe ions were identified in octahedral positions and Ni ions in tetrahedral positions, confirming the spinel structure. The $CoFe_2O_4$ NPs also presented results of a spinel-type material with Fe and Co present in tetrahedral and octahedral positions for the samples heat treated at 250 °C and the samples heat treated at 800 °C with Fe present in tetrahedral and octahedral positions. The results of cytotoxicity testing of $NiFe_2O_4$ and $CoFe_2O_4$ NPs with erythrocytes and leukocytes demonstrate no significant differences compared to the control test, which suggest the hemocompatible properties of the materials. Among the concentrations of $NiFe_2O_4$ and $CoFe_2O_4$ solutions assessed in this study, we tested the 8 mg/ml which was considered high when compared to the concentrations evaluated in other studies. Another relevant point of these compatibility results with erythrocytes and leukocytes is the application of *in vivo* tests, thus reducing the number of animals used in the experiment.

Declarations

Conflict of interest On behalf of all authors, the corresponding author states that there is no conflict of interest.

References

1. Pankhurst QA, Connolly J, Jones SK, Dobson (2003) Applications of magnetic nanoparticles in biomedicine. J of Phys D: Appl Phys 36:R167–R181 **()**
2. Capeletti LA, Oliveira LF, De, Gonçalves KA, Oliveira JFA, De, Saito A, Kobarg J, Santos JHZ, Dos, Cardoso MB (2014) Tailored Silica–Antibiotic Nanoparticles: Overcoming Bacterial Resistance with Low Cytotoxicity. Langmuir 30:7456–7464 **()**
3. Li J, Lin Y, Liu X, Zhang Q, Miao H, Zhang T, Wen B (2011) The study of transition on $NiFe_2O_4$ nanoparticles prepared by co-precipitation/calcinations. Phase Transitions 84:49–57
4. Chun J, Seo SW, Jung GY, Lee J (2011) Easy access to efficient magnetically recyclable separation of histidine-tagged proteins using superparamagnbetic nickel ferrite nanoparticle clusters. J of Materials Chemistry 21:6713–6717 **()**

5. Momin N, Deshmukh A, Radha S (2015) Synthesis and characterization of $CoFe_2O_4$ & $NiFe_2O_4$ magnetic nanoparticles for various biomedical applications: cell viability and cell death evaluations. J of Nano Research 34:1–8
6. Rogach AL, Talapin DV, Shevchenko EV, Kornowski A, Haase M, Weller H (2002) Organization of Matter on Different Size Scales: Monodisperse Nanocrystals and Their Superstructures. Advanced Funcional Materials 12:653–664
7. Amiri M, Pardakhti A, Ahmadi-Zeidabadi M, Akbari A, Salavati-Niasari M (2018) Magnetic nickel ferrite nanoparticles: Green synthesis by Urtica and therapeutic effect of frequency magnetic field on creating cytotoxic response in neural cell lines. Colloids Surf B 172:244–253
8. Polarz S, Neues F, Van den Berg MWE, Grüner W, Khodeir L (2005) Mesosynthesis of Zn-O-Silica Composites for Methanol Nanocatalysis. J of the American Chemical Society 127:12028–12037
9. Wang WP, Yang H, Xian T, Jiang JL (2012) XPS and Magnetic Properties of $CoFe_2O_4$ Nanoparticles Synthesized by a Polyacrylamide Gel Route. Mater Trans 53(9):1586–1589
10. Bader SD (2006) Colloquium: Opportunities in nanomagnetism. Rev Mod Phys 78:1–15
11. Wood RW, Miles J, Olson T (2002) Recording technologies for terabit per square inch systems. Magnetics IEE Transactions 38:1711–1718
12. Chen DH, Chen YY (2001) Synthesis of Barium Ferrite Ultrafine Particles by Coprecipitation in the Presence of Polyacrylic Acid. J Colliod Interface Sci 235(1):9–14
13. Amiri M, Abari A, Ahmadi M, Pardahti A, Salavati-Niasari M (2018) Synthesis and in vitro evaluation of a novel magnetic drug delivery system; proecological method for the preparation of $CoFe_2O_4$ nanostructures. J Mol Liq 249:1151–1160 **()**
14. Sanadi KR, Patil SP, Helavi VB (2018) Effect of Cobalt Substitution on Thermoelectrical and Magnetic Properties of Copper Ferrites Synthesized by Simple Sol-Gel Method. Advanced Porous Materials 6(1):28–34
15. Azevedo RB, Silva LP, Lemos APC, Bao SN, Lacava ZGM, Safarik I, Safarikova M, Morais PC (2003). IEEE Transactions on Magnetics 39:2660
16. Auffan M, Rose J, Orsiere T, De Meo M, Thill A, Zeyons O et al (2009) CeO_2 nanoparticles induce DNA damage towards human dermal fibroblasts in vitro. Nanotoxicology 3:16171
17. Park EJ, Choi J, Park YK, Park K (2008) Oxidative stress induced by cerium oxide nanoparticles in cultured BEAS2B cells. Toxicology 245:90–100
18. Saikia H, Hazarika KK, Chutia B, Choudhury B, Bharali P (2017) A Simple Chemical Route toward High Surface Area CeO2 Nanoparticles Displaying Remarkable Radical Scavenging Activity. Chemistry Select 2:3369–3375
19. Martinez MJS, Rahme K, Corbalan JJ, Holmes JD, Taiber L, Medina C, Radomski MW (2014) Pegylation Increases Platelet Biocompatibility of Gold Nanoparticles. J Biomed Nanotechnol 10:1004–1015
20. Amiri M, Salavati-Niasari M, Pardakhty A, Ahmadi M, Akbari A (2017) Caffeine: A novel green precursor for synthesis of magnetic $CoFe_2O_4$ nanoparticles and pH-sensitive magnetic alginate beads for drug delivery. Materials Science Engineering: C 76:1085–1093 **()**
21. Bohara RA, Thorat ND, Yadav HM, Pawar SH (2014) One-step synthesis of uniform and biocompatible amine functionalized cobalt ferrite nanoparticles: a potential carrier for biomedical applications. New J Chem 38:2979–2986
22. Kückelhaus S, Garcia VAP, Lacava LM, Azevedo RB, Lacava ZGM, Lima ECD, Figueiredo F, Tedesco AC, Morais PC (2003) Biological investigation of a citrate-coated cobalt–ferrite-based magnetic fluid. J Appl Phys 93:6707
23. Kückelhaus S, Reis SC, Carneiro MF, Tedesco AC, Oliveira DM, Lima ECD, Morais PC, Azevedo RB, Lavaca ZGM (2004). J. Magn. Magn. Materials **272–276**:2402–2403
24. Kückelhaus S, Tedesco AC, Oliveira DM, Morais PC, Boaventura GR, Lavaca ZGM (2005) Optical emission spectroscopy as a tool for the biodistribution investigation of cobalt-ferrite nanoparticles in mice. J Appl Phys 97:10Q910 **()**
25. Aragon FH, Coaquira JAH, Villegas-Lelovsky L, Silva SW da, Cesar DF, Nagamine LCCM, Cohen R, Menendez-Proupin E, Morais PC (2015) Evolution of the doping regimes in the Al-doped SnO2 nanoparticles prepared by a polymer precursor method. J Phys: Condens Matter 27:095301
26. Fontanive VCP (2012) Síntese, caracterização e análises in vitro e. In: vivo da toxicidade de nanopartículas de ferrita de cobalto para aplicações biomédicas. Dissertação de mestrado. Pós Graduação em Ciências Farmacêuticas. Universidade Estadual do Centro Oeste
27. Gonçalves NS (2013) Síntese e caracterização de nanopartículas de ferritas de níquel e de cobalto preparadas pelo método sol-gel-protéico. Tese de Doutorado. Universidade Federal do Ceará
28. Bezerra DC, Fernandes PC, Silva TRG, Araujo EM, Costa ACFM (2010). Polímeros 20(5):389–394 **()**
29. Zabotto FL, Gualdi AJ, Eiras JA, Oliveira AJA, De, Garcia D (2012) Influence of the Sintering Temperature on the Magnetic and Electric Properties of $NiFe_2O_4$ Ferrites. Mat Res 15(3):428–433
30. Hoyos JRM, Zabotto FL, Garcia D, Kiminami RHG (2013) Microwave sintering of nickel ferrite synthesized by the Pechini method. Cerâmica 59(351):360–365
31. Amiri M, Salavati-Niasari M, Akbari A, Gholami T (2017) (**2017**) **24846**–**24860**
32. Franco A, Machado FLA, Zapf VS (2011) Magnetic properties of nanoparticles of cobalt ferrite at high magnetic field. J Appl Phys 110:053913 **()**
33. Sawatsky GA, Woude FV, De, Morrish A (1969) Mössbauer Study of Several Ferrimagnetic Spinels Phys. Rev 187:747–757 **()**
34. Zhao DF, Yang H, Xian T, Wang WP, Wei Zq, Li RS, Feng WJ, Jiang JL (2013) Preparation and Properties of $NiFe_2O_4$ Nanoparticles by a Polyacrylamide Gel Route. J of Synthetic Crystals 42(2):316–322
35. Fujii T, Groot FMF, Sawatzky GA, Voogt FC, Hibma T, Okada K (1999) In situ XPS analysis of various iron oxide films grown by NO2-assisted molecular-beam epitaxy. Phys RevB Condensed Matter Materials Physics 59:3195–3202
36. Sagadevana S, Chowdhuryb ZZ, Rafiquec RF (2018) Preparation and Characterization of Nickel ferrite Nanoparticles via Co-precipitation Method. Materials Research 21(2):e20160533
37. Biesingera MC, Payne BP, Grosvenord AP, Laua LWM, Gersonb AR, Smart RSC (2011) Resolving surface chemical states in XPS analysis of first row transition metals, oxides and hydroxides: Cr, Mn, Fe, Co and Ni. Appl Surf Sci 257:2717–2730
38. Yoon H,. et al (2013) Synthesis, microstructure, and magnetic properties of monosized MnxZnyFe3 – x – yO4 ferrite nanocrystals. Nanoscale Res Lett 8:530
39. Ali IA et al (2017) Determination of concentrations of Fe, Mg, and Zn in some ferrite samples using neutron activation analysis and X-ray fluorescence techniques. Applied Radiation Isotipes 122:63–67
40. Neuberger T, Schöpf B, Hofmann H, Hofmann M, Von Rechenberg B (2005) Superparamagnetic nanoparticles for biomedical applications: Possibilities and limitations of a new drug delivery system. J of Magnetism Magnetic Materials 293:483–496
41. Singh HS, Sangwa N (2017) International Journal of Engineering Science Invention 6(10):36–39
42. Houshiar M, Zebhi F, Razi ZJ, Alidoust A, Askari Z (2014) Synthesis of cobalt ferrite ($CoFe_2O_4$) nanoparticles using combustion, coprecipitation, and precipitation methods: A comparison study

of size, structural, and magnetic properties. J Magn Magn Mater 371:43–48
43. Cunha SS (2014) Aplicação de Nanopartículas Magnéticas em Hipertermia. Dissertação de mestrado. Escola Superior de Tecnologia e Gestão Instituto Politécnico de Bragança
44. Amiri M, Salavati-Niasari M, Akbari AA (2017). Microchim Acta 184:825–833 **()**
45. Amiri M, Salavati-Niasari M, Abari A, Razavi R (2017). J. of Materials Science: Materials in Electronics **28 10495–10508**
46. Khojasteh H, Amiri M, Sohrabi A, Khanahmadzadeh S, Salavati-Niasari M, Moayedi H (2020). Journal of Materials Research Technology 9(2):1380–1388 **()**
47. Cotica LF, Freitas VF, Dias GS, Santos IA, Vendrame SC, Halil NM, Mainardes RM, Staruch M, Jain M (2012) Simple and facile approach to synthesize. J of Magnetism Magnetic Materials 324:559–563
48. Özçelik S, Yalçın B, Arda L, Santos H, Sáez-Puche R, Angurel LA, Fuente GF de la, Özçelik B (2021) Structure, magnetic, photocatalytic and blood compatibility studies of nickel nanoferrites prepared by laser ablation technique in distilled water. J of Alloys Compounds 854:157279
49. Vendrame SC (2011) Síntese, caracterização e análise de citotoxidade de nanopartículas de magnetita para aplicações biomédicas. Dissertação (Mestrado) – Ciências Farmacêuticas. Universidade Estadual do Centro Oeste, Guarapuava
50. Hankare PP, Sanadi KR, Garadkar KM, Patil DR, Mulla IS (2013) Synthesis and characterization of nickel substituted cobalt ferrite nanoparticles by sol-gel auto-combustion method. J of Alloys Compounds 553:383–388
51. Cotica LF, Freitas VF, Silva DM, Honjoya K, Santos IA, Fontanive VCP, Khalil NM, Mainardes RM, Kioshima ES, Guo R, Bhalia AS (2014) Thermal Decomposition Synthesis and Assessment of Effects on Blood Cells and In Vivo Damages of Cobalt Ferrite Nanoparticles. J of Nano Research 28:131–140